JSAE 20249074 / SAE 2024-32-0074

3D-CFD simulations of H2 ICEs: a preliminary evaluation of a laminar flame speed correction for thermo-diffusive instability

Stefano Sfriso[1], Fabio Berni[1], Sebastiano Breda[1], Stefano Fontanesi[1], Ilario Cordisco[1], Caio Ramalho Leite[2], Pierre Brequigny[2], Fabrice Foucher[2]

[1]Università degli studi di Modena e Reggio Emilia, [2]Université d'Orléans

ABSTRACT

In recent years, climate change and geopolitical instability have intensified the focus on sustainable power generation. This shift seeks alternatives that balance environmental impact, cost-effectiveness, and practicality. Specifically, in transportation and power generation, electric motors face challenges against internal combustion engines due to the high cost and mass of batteries required for energy storage. This makes electric solutions less favorable for these sectors. Conversely, internal combustion engines, when properly fueled, offer cost-effectiveness and a quasi-environmentally-neutral option. To address these challenges, researchers have explored e-fuels derived from renewable sources as a carbon-neutral supply for internal combustion engines. Among these, hydrogen is particularly promising. In hydrogen-powered internal combustion engines, 3D-CFD (Computational Fluid Dynamics) in-cylinder models are crucial. Once validated, these models can speed up the design process. A key challenge in simulating H2 combustion is accurately representing flame thermo-diffusive instabilities in lean mixtures, which are vital for peak engine efficiency. Accurate representation of the combustion process under lean conditions is thus mandatory in 3D-CFD models. This study represents a preliminary effort to incorporate thermo-diffusive instabilities into a 3D-CFD in-cylinder framework. An extensively validated numerical framework was modified to include instability-induced acceleration in flame propagation speed. The outcomes were analyzed and compared with results obtained without the correction term. Although improvements were limited to certain operating conditions, the study underscored the importance of considering the influence of turbulence on instability.

INTRODUCTION

Research on H_2 internal combustion engines (ICEs) relies on both experimental and numerical activities. On the experimental side, Leite et al. [1] focused on the analysis of ultra-lean H_2 combustion, with particular attention in the description of the combustion initiation. Other researchers [2], [3] explored NO_x emissions at different operating conditions. Tsujimura and Suzuki [4] carried out a mixed numerical/experimental investigation to develop a large hydrogen-fueled engine for stationary operation, while Luo et al. [5] concentrated on the calibration of turbocharged hydrogen engines, aiming at obtaining an optimal balance between adiabatic efficiency and turbocharger energy recovery.

As for the numerical activities and, in particular, focusing the attention on 3D-CFD combustion simulations, many of the works available in literature are purely numerical explorations, not supported by experimental data for the validation. From a modeling standpoint, both flamelet and detailed chemistry approaches are adopted. Maio et al. [6] correlated 3D-CFD results with experimental data using the ECFM model, at the cost of case-by-case combustion model calibration. Berni et al. [7] carried out a numerical investigation on performance, emissions, knock, and heat transfer of an internal combustion engine fueled with pure NH_3, pure H_2 and mixtures of the two. In [7], G-equation along with detailed chemistry for the evaluation of the burnt gas composition are employed and a correlation for unstretched laminar flame speed is adopted for simplicity. Similarly, Hernandez et al. [8] simulated ultra-lean H_2 combustion using G-equation and detailed chemistry was adopted for the computation of laminar flame speed. Moreover, in [8], a correction factor for the flame instability was included. Other authors addressed the simulation of H_2 combustion with approaches based on pure detailed chemistry. For example, Liu et al. [9] and Babayev et al. [10] employed the SAGE model for H_2 TJI combustion and H_2 compression ignition combustion, respectively.

The significance of 3D-CFD lies in its ability to investigate parameters difficult to measure experimentally. Once validated, CFD accelerates engine development and optimization. However, in order to benefit of such advantages, the evaluation of both accuracy and reliability of the 3D-CFD model is required. This study exploits the 3D-CFD framework for combustion simulations of H_2 ICEs already adopted by the authors in previous papers [11], [12], [13]. Specifically, the numerical setup utilizes the G-equation combustion model, Verhelst correlation for the laminar flame speed and a Damköhler derived correlation for the turbulent flame speed. Compared to the previous papers, the novelty of the present work relies on the inclusion of the thermo-diffusive instability effects typical of lean/ultra-lean operating conditions. In particular, the behavior of the framework is compared with and without thermo-diffusive effects. For a proper evaluation of the CFD framework,

experiments carried on a PSA EP6 optical engine are available. The numerical-experimental comparison is made at fixed engine speed and spark timing, and at two different equivalence ratios, namely 0.3 and 0.55. Interestingly, compared to a previous activity by the authors on a direct injection H_2 ICE [11], [13], in the present study a continuous PFI strategy ensuring homogeneous mixtures is adopted. This eliminates the uncertainties on injection and mixing and allows the attention to be focused on the combustion, and in particular on the effect of the hydrogen thermo-diffusive instability.

In the following, the paper describes the investigated engine and the experimental apparatus. Then, the numerical framework is detailed, and the main CFD outcomes are presented. CFD prediction errors are addressed and commented. Finally, conclusions are drawn and both predictive capabilities and limitations of the model are pointed out.

EXPERIMENTAL APPARATUS

The investigated engine is a four-valve spark-ignition optical unit, with tumble-inducing intake ducts. The main specifications are listed in Table 1. The entire test bench layout is shown in Fig.1. The most relevant quantities are monitored by the illustrated sensors. Instantaneous in-cylinder pressure traces are recorded at each cycle and their average over 100 consecutive cycles is utilized in the 3D-CFD URANS simulations for comparison. Then, instantaneous intake and exhaust plenum pressures are measured and their ensemble-averages are used as boundary conditions for the simulations. Cycle-averaged temperatures at intake and exhaust plenums are recorded and adopted as boundary conditions for the CFD analyses. Mass flow controllers regulate the hydrogen-air mixture upstream the intake plenum.

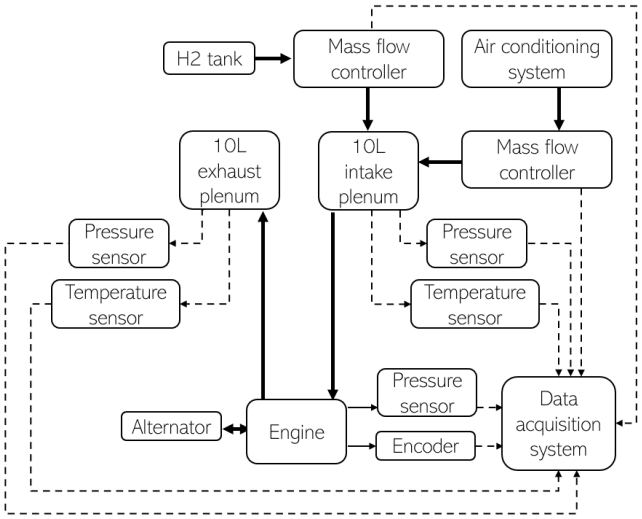

Figure 1. Test bench scheme. [13]

The experimental setup includes intake and exhaust pipes as well as plenums, as visible in Fig. 2. To ensure mixture homogeneity, hydrogen is continuously injected through a 6 mm pipe positioned as distant as possible from the intake valve along the duct (near the intake plenum). Comprehensive details of the experimental setup are provided in [1]. Additionally, the length of the ducts is adequate to attenuate macro turbulent structures emerging at the junction between the plenum and intake pipe.

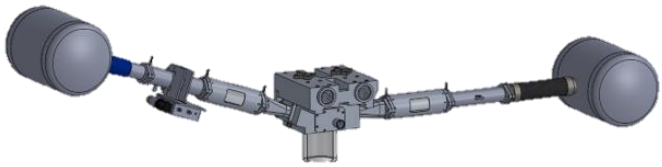

Figure 2. Single-cylinder engine with intake/exhaust plenums and ducts [1].

Table 1. Stock engine characteristics.

N° of cylinders	1
Bore	77 mm
Stroke	85.8 mm
Displacement	400 cm^3
Compression ratio	10.5:1
Connecting rod length	138.5 mm
Pin offset	0.8 mm
N° of valves	4
Injection	PFI
Combustion initiation	SI

The optical piston is designed to mimic the original piston shape while accommodating a quartz window installation, as visible in Fig. 3. A dedicated spark plug featuring three mass electrodes, shown in Fig. 4, is purposely selected for hydrogen operations and it is utilized in place of the original spark plug. The selection is based on the author's experience with various engine types. Bosch ZLR07MTE exhibits in fact the optimal balance between reduction of cycle-to-cycle variability at low loads and extension of the limit of abnormal combustion at high loads.

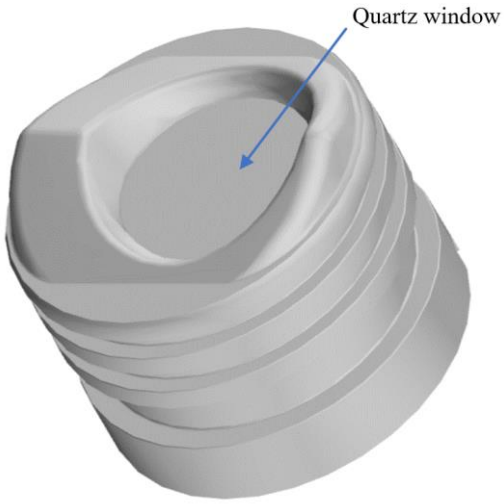

Figure 3. Optical piston.

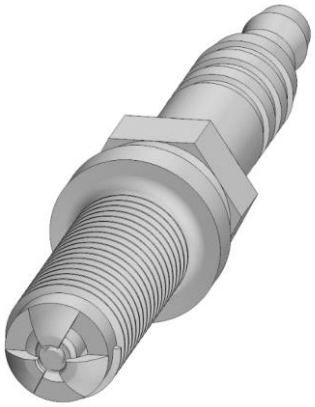

Figure 4. Spark plug for hydrogen operation. [13]

As previously mentioned, the experimental data for the present study are obtained at fixed engine speed and spark timing, while varying the equivalence ratio. Details of the investigated cases are summarized in Table 2.

Table 2. Experimental operating conditions considered for the numerical simulations.

φ	Ignition [° CA BTDC]	Intake temperature [K]	Exhaust temperature [K]	Average intake pressure [bar]	rpm	CoV IMEP [%]
0.3	-15	296	596	0.7	1500	4.875
0.55	-15	296	666	0.7	1500	1.508

3D-CFD MODEL

The physical setup is very similar to the one used in previous studies [11], [12], [13] and it is briefly summarized below. Simulations are carried out by STAR-CD, licensed by SIEMENS DISW. Turbulence is addressed via the k-ε RNG model [14], [15], extensively adopted by the authors in the past [16], [17]. The time-step is 0.05° CA (=5.55×10^{-6} s at 1500 rpm) during valve motion, ignition and combustion. Otherwise, it is 0.1° CA (=1.11×10^{-5} s at 1500 rpm). The Improved GruMo-UniMORE model [18], [19] implemented in STAR-CD is here adopted and it is able to consider the actual Prandtl number of the hydrogen mixture and to eliminate the solution dependence on the near-wall grid resolution.

Ignition

The URANS ignition model is derived from a LES version [20] validated in the past by the authors. It has a similar approach to Herweg and Maly [21] one, i.e. it covers the initial kernel stage governed by unstretched laminar flame speed, gas expansion between electrodes and local heat conduction. Eq. 1 expresses the kernel radius growth and it is derived from first law of thermodynamics and ideal gas law.

$$\frac{dr_k}{dt} = \frac{\rho_u}{\rho}(Sl + S_{cond}) + \frac{V_k}{A_k}\left[\frac{1}{T_k}\frac{dT_k}{dt}\right]$$

(1)

In Eq. 1, r_k denotes the kernel radius, ρ_u is the unburnt density, ρ represents the density, Sl stands for the laminar flame speed, T_k is the average kernel temperature and, finally, A_k and V_k are area and volume of the kernel, respectively. S_{cond} is a contribution related to the heat conduction from the plasma column formed between the electrodes. In order to express S_{cond}, a methodology derived from the one introduced in [22] is adopted. Specifically, a dimensionless wave equation is formulated to represent the temperature increase near the ignition point resulting from heat conduction and it is expressed by Eq. 2.

$$\rho c_p \frac{\partial T}{\partial t} = \frac{\partial}{\partial x}\left(k\frac{\partial T}{\partial x}\right) + S$$

(2)

c_p and T represent the specific heat at constant pressure and the temperature of the gas, respectively. t, x, k and S stand for time, space coordinate, thermal conductivity and source term. In this investigation, product ρc_p and thermal conductivity are fixed to 8000 J/(m^{3}K) and 0.2 W/(mK). The boundary condition of Eq. 2 is the plasma temperature at the spark. Once Eq. 2 is solved, the flame position is determined as the distance between spark and point where the temperature reaches the adiabatic flame temperature. The velocity S_{cond} is then determined as flame position variation over the time.

The solver computes the equivalent flame kernel radius according to Eq. 1 until it reaches a threshold value, that in this activity is set to 2.3 mm. After this value, the combustion model is switched on while the ignition one is turned off. The value for the transition between the models de facto acts as a filter for the turbulence scales. Below that size, the scales of turbulence are supposed not capable to interact with the small flame to enhance the propagation, thus turbulence is not accounted for the kernel growth. Moreover, for the very early stage of the kernel development, the unstretched laminar flame speed is considered and the thermo-diffusive instability is neglected. In fact, according to [23], its influence is observed only after a certain kernel size. In particular, Bradley shows that, at φ=0.5, 10 bar and 365 K, the radius at which the effect of the instability becomes relevant is 0.5 mm on average. Moreover, it is observed that, increasing pressure or decreasing equivalence ratio, the radius further decreases. The trend with temperature is not shown. In the computations presented in the current work, the ignition occurs at 11.3 bar and 772 K, for equivalence ratios of 0.3 and 0.55. The huge difference in temperature makes the assessment of the instability onset at the present conditions difficult. However, as it will be shown later, temperature has a stabilizing effect on the flame. For this reason, the adoption of a switch radius equal to 2.3 mm and neglecting the instability effect up to that size can be considered reasonable.

The initial condition of Eq. 1 is represented by a kernel radius equal to 0.2 mm, a suitable size to represent a sphere with a volume three times that of the plasma channel. The plasma channel is assumed to be a cylinder with a height equal to the spark gap and a radius equal to the flame thickness. The multiplication by 3 for the calculation of the volume is necessary to account for the presence of 3 electrodes in the spark, with each spark gap measuring 0.6 mm in height.

This approach for the calculation of the initial kernel radius is inherited from [11], [12], [13] and it relies on chemical kinetic computations carried out in DARS2020 using Konnov mechanism [24], being the same on which the employed laminar flame speed correlation is based. Specifically, chemical kinetic computations are used to determine the laminar flame thickness as specified in [25] and they are carried out at pressure, temperature and equivalence ratio present at the spark timing inside the cylinder. For both the simulated cases, the computed values led to an estimation of early first kernel size around 0.2mm.

Combustion

Combustion is modelled by G-equation, where laminar and turbulent flame speeds are determined using Verhelst correlation [26] and a Damköhler derived expression [27], [28], [29] respectively. Verhelst correlation is derived from chemical kinetics computations based on Konnov [30] mechanism and is validated at high pressures. However, it does not incorporate flame acceleration resulting from thermo-diffusive instability. Verhelst correlation is valid for p, T, φ and EGR ranges reported hereafter: 5bar≤p≤45bar, 500K≤T≤900K, 0.33≤φ≤5, and 0%≤EGR≤50%. The turbulent flame speed is determined using the Damköhler derived correlation reported in Eq. 3.

$$S_T = Sl\left(1 + A \cdot KGF \cdot \left(\frac{u'}{Sl}\right)^{\frac{5}{6}}\right)$$

(3)

Sl is the laminar flame speed and u' is the root-mean-square of the turbulent velocity fluctuations. A is an empirical coefficient set to 3.3 in the present study, after an extensive validation of this correlation in previous activities [11], [12], [13].

Thermo-diffusive instability

The flame instability due to thermo-diffusive effects is a widely discussed topic in research on hydrogen ICEs. It arises from the disparity between molecular diffusivity of hydrogen in an air mixture and thermal diffusivity, causing flame acceleration in stretched regions where reactant transport outpaces the cooling associated to the temperature gradient increase. Consequently, in a thermo-diffusive unstable flame, wrinkling is a self-promoting process, leading in turn to an augmented flame speed. Despite the thermo-diffusive instability influence seems clearly affirmed in laminar flames, for turbulent flames under pressure and temperature conditions typical of internal combustion engines is still not. In this regard, the present paper includes the effect of thermo-diffusive instability in order to investigate the impact at engine-like conditions. Such instability is accounted for based on the practice presented in the following.

In Matalon work [31], the thermo-diffusive instability is investigated by means of the linear stability analysis of a planar flame in the context of the hydrodynamic theory. With this theoretical analysis it is possible to infer the influence of the instability under various pressure, temperature and equivalence ratio conditions, as suggested by Howarth in [32]. Thanks to the extension of same theory to 3D domains as proposed again by Howarth in [33], a correlation between unstretched laminar flame speed Sl and the one measured by DNS simulations Sl_{corr} (that naturally includes instability phenomena) is obtained. Such a correlation is proposed in Eq. 4.

$$\frac{Sl_{corr}}{Sl} = \begin{cases} e^{0.08\omega_2} & if\ \varphi > \varphi_{lim} \\ 1 + 0.47\omega_2 & if\ \varphi < \varphi_{lim} \end{cases}$$

(4)

In order to explain the meaning of ω_2 and how to calculate it, the analytical expression of the instability wave growth rate (up to the second order) is recovered from [31] and reported in Eq. 5.

$$\omega = \omega_{DL} Sl\kappa - \delta_l\left[B_1 + \beta\left(Le_{eff} - 1\right)B_2 + PrB_3\right]Sl\kappa^2$$

(5)

ω is the instability wave growth rate, ω_{DL} the first order term of wave growth rate (representing the hydrodynamic instability), κ the local flame curvature, δ_l the laminar flame thickness, β the Zel'dovich number, Le_{eff} the effective Lewis number of the mixture, computed according to reference [31] and Pr the mixture Prandl number. B_1, B_2 and B_3 are coefficients whose computation is reported in [31]. The opposite of the term in the square brackets is ω_2 assumed by Howarth to be representative of the thermo-diffusive instability. In order to compute Zel'dovich number, the activation energy of hydrogen oxidation is needed and the method proposed by Law and Sung [34] is employed. A map in the pressure-equivalence ratio space for three temperatures is reported in Fig. 5, showing area and intensity of thermo-diffusive instability influence. The temperatures for the proposed maps are representative of the average unburnt temperature present in the cylinder during combustion for all the examined cases.

$\varphi_{lim} = (0.3475 - 0.000325 \cdot T) \cdot p^{0.1425+0.000225 \cdot T}$ is the limit equivalence ratio, for a fixed pressure and temperature, governing the switch between the two correlations of Eq. 4 for the laminar flame speed correction. φ_{lim} expression is empirical and it expresses the position of the maximum values of ω_2 in the maps of Fig. 5. In other words, it splits the two regions where the two correlations are found [33].

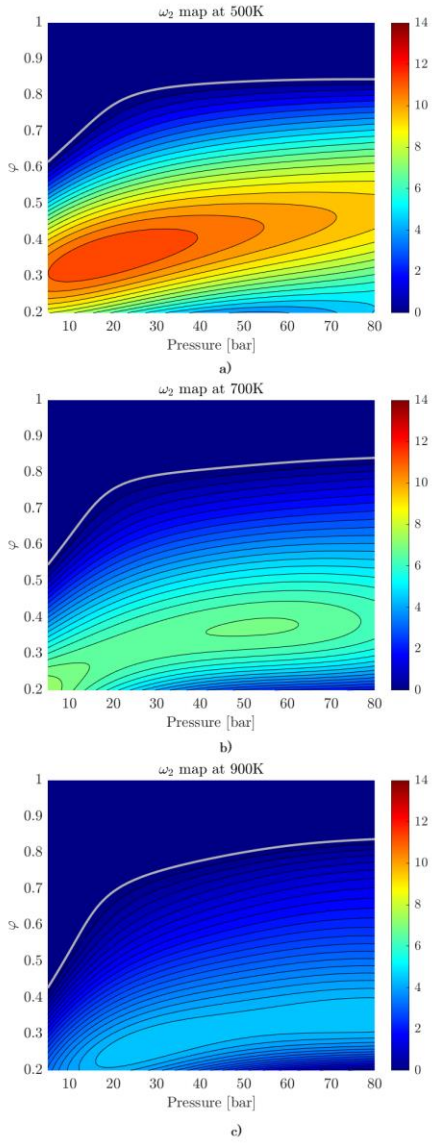

Figure 5. ω_2 maps in the p-φ space at 500 K a), 700 K b) and 900 K c). The grey line separates the stable area (upper left corner) and the unstable one (lower right corner).

One important aspect which is not accounted for in the argumentation proposed above is the interaction between turbulence and unstable laminar flame. It is scarcely addressed even in literature. Matalon et al. [35], [36] noticed that, for increasing turbulence intensity, flame instabilities tend to be overcome by turbulent wrinkling. In [37], [38], Bradley proposed a way to generally quantify the relative influence of wrinkling induced by laminar effects and turbulent ones, introducing a parameter called the Karlovitz stretch factor. Following Bradley formulation, the mentioned factor is computed as in Eq. 6.

$$K = 0.25 \cdot \left(\frac{u'}{Sl}\right)^2 \cdot {R_l}^{-0.5} \quad (6)$$

u' represents the root mean square (rms) of the turbulent velocity fluctuations and it is calculated as $\sqrt{\frac{2}{3}tke}$, where tke denotes the turbulent kinetic energy. Sl stands for the laminar burning velocity and R_l is the turbulent Reynolds number. The latter is determined as $\frac{u' l_t}{\nu}$, where l_t represents the integral length scale and ν is the dynamic viscosity.

In [37], Bradley et al. asserted that when the Karlovitz number (K) is less than or equal to 0.05, flame instability effects become significant. Moreover, in a subsequent study [38], the same authors delineated the "regime of mild turbulence and laminar instabilities" for $K \leq 0.1$ and identified the "fully turbulent regime" for $K > 0.1$. Essentially, when K is below 0.1, instability effects are non-negligible. Conversely, above 0.1 and with increasing K values, turbulence dominates and intensifies flame wrinkling, making the influence of thermo-diffusive induced wrinkling negligible.

Boundary conditions

At the inlet boundary, a uniform mixture of the desired composition is imposed. Throughout the simulation, intake and exhaust pressure boundary conditions are applied as time-varying traces, as illustrated in Fig. 6. Additionally, temperatures at inlet and outlet are set as constant values and equal to cycle averages, as the time-dependent ones are not available. Values are reported in Table 2 for each equivalence ratio.

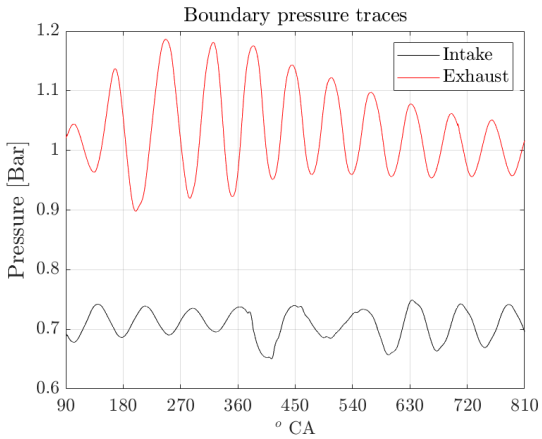

Figure 6. Example of time-dependent boundary conditions imposed at intake and exhaust. The reported traces refer to the φ=0.3 case.

Wall temperatures are set based on authors' experience on heat transfer analyses of both spark ignition and compression ignition engines [39] and they are listed in Table 3. Temperatures are different in the two cases in order to mimic the increase of heat rejection with φ. In particular, in the φ=0.55 case, all the walls are 70 K hotter than in the φ=0.3 one, following the same trend in temperature observed in Fig. 7 for the exhaust plenum. This approximate (but effective) method for the wall temperature estimations is necessary as not enough data are available to carry out a detailed CHT analysis of the engine. To assess the validity of the method, φ=0.55 case is run with the same wall temperatures of the φ=0.3 one, leading to the intake air mass flow prediction shown by the black circle in Fig 8, which is a strong overestimation of the experimental datum. Instead, the corrected wall temperatures (reported in Table 3) are capable to improve the prediction of the air mass flow, leading to a

value closer to the experimental counterpart (red cross vs blue one in Fig. 8). For clarity, the intake mass flow rate for the φ=0.3 case is not affected. In fact, in the light of the satisfying agreement with the experiment, no correction is actually considered. Then, this case is assumed as reference and, moving to φ=0.55, wall temperatures are modified as discussed above.

Table 3. Wall temperature values for the cylinder boundaries.

Domain surface	φ=0.3	φ=0.55
Combustion dome	420K	490K
Piston crown	420K	490K
Cylinder wall	390K	460K
Intake valve stem and port	320K	390K
Intake valve face	350K	420K
Exhaust valve stem	640K	710K
Exhaust valve face	640K	710K
Exhaust port	600K	670K
Spark plug	500K	570K

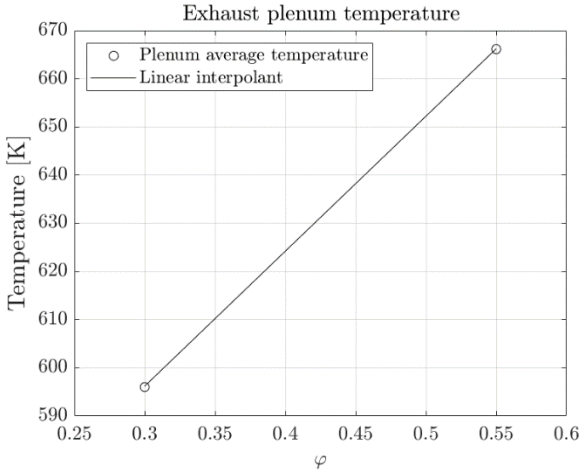

Figure 7. Cycle-average temperature recorded in the exhaust plenum for the different operating conditions.

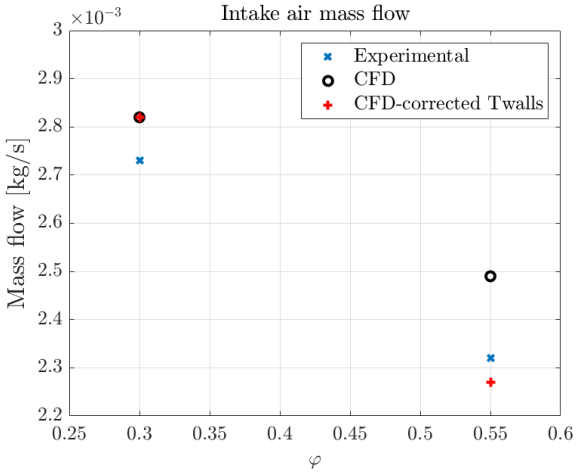

Figure 8. Intake air mass flow comparison between CFD and experiments.

Mesh

In order to select the computational grid, a mesh sensitivity analysis is conducted using the φ=0.55 case. Two different grids are tested. The first one is a coarse mesh representing a balance between accuracy and computational efficiency, referred to as "Coarse mesh" in the following. The second is a finer version, referred to as the "Fine mesh". The former has a minimum cell size of 0.6 mm and a maximum of 1.2 mm, while the latter features minimum and maximum cell sizes equal to 0.4 mm and 0.8 mm, respectively. At the Bottom Dead Center (BDC), the finer version has nearly 1 million cells, whereas the coarse grid has roughly 500 k cells. As illustrated in Fig. 9, halving the cell number has not a significant impact in the predicted in-cylinder pressure. Therefore, the coarser mesh is preferred to save computational cost and time.

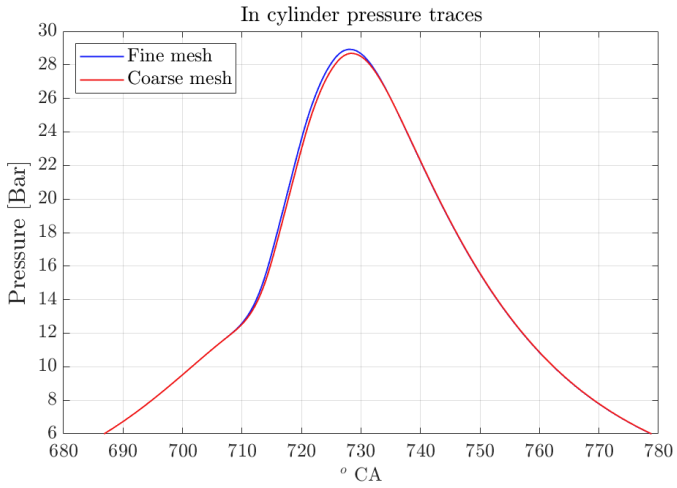

Figure 9. Pressure traces computed with different grids. [13]

The computational mesh adopted for the simulations is depicted in Fig. 10. Cell size varies within the prescribed minimum and maximum values (0.6 and 1.2 mm) based on the local geometry. Specifically, around the spark plug, the cell size is halved. Along the walls, one prismatic layer with a height of 0.3 mm is employed.

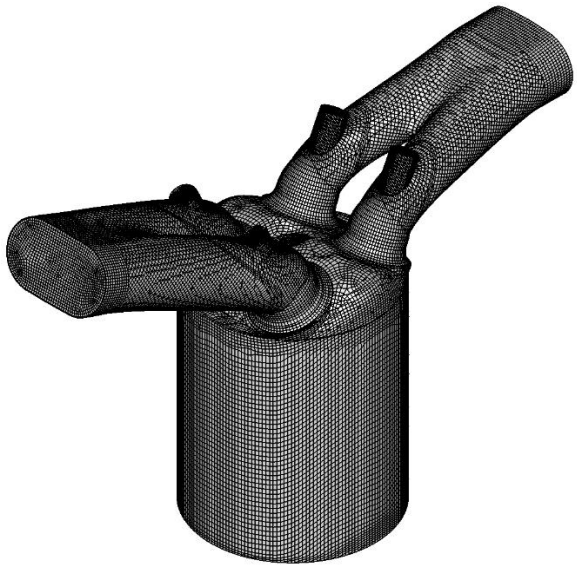

Figure 10. The adopted computational grid at the BDC. [13]

RESULTS

Except for the thermo-diffusive instability, the rest of the numerical setup described above was already employed by the authors in previous activities, on a completely different H_2 engine [11], [12] as well as on the same engine here investigated [13]. In this regard, the results presented in Fig. 11 are obtained on the currently analyzed power-unit without considering the instability. All the relative details are presented in reference [13]. In the current work, the same setup is adopted, but with the correction factor based on ω_2. The maps of ω_2 computed at three temperatures and reported in Fig. 5 are interpolated with a polynomial function of pressure, equivalence ratio and temperature which is implemented in the code. Therefore, for each computational cell involved in combustion, based on the local conditions, both laminar flame speed and ω_2 are computed (by Verhelst correlation and the polynomial function mentioned above, respectively). Then, by Eq. 5, the corrected laminar flame speed is calculated and it is exploited in Eq. 3 to evaluate S_T, which is exploited in turn by G-Equation. The pressure traces obtained by the inclusion of the thermo-diffusive instability effect are presented in Fig. 11 and compared to experimental ones.

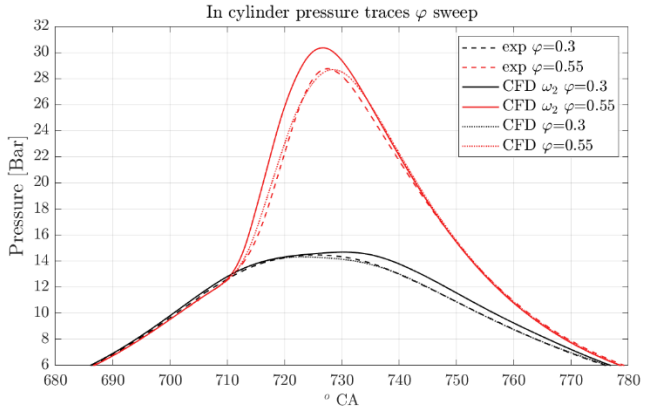

Figure 11. Numerical (dotted), numerical corrected with ω_2 parameter (solid) and experimental (dashed) pressure traces.

Both the pressure traces appear to be affected by the correction. The combustion is faster in all the cases, leading to higher pressure peaks. To have a better understanding of the combustion development, the apparent heat release rate is computed with the same method for both experimental and numerical pressure traces. In Fig. 12, the comparison between numerical and experimental traces is reported for both original (dotted) and corrected (solid) cases.

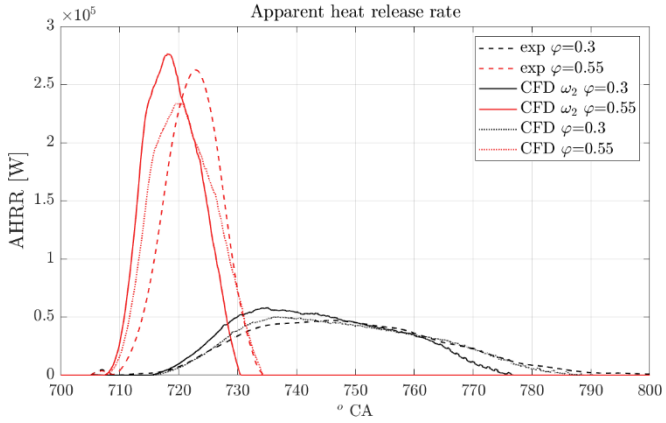

Figure 12. Numerical and experimental apparent heat release rate for the original framework and the one including the instability effect.

Integrating each curve and normalizing by the respective maxima, the burnt mass profiles reported in Fig. 13 can be inferred.

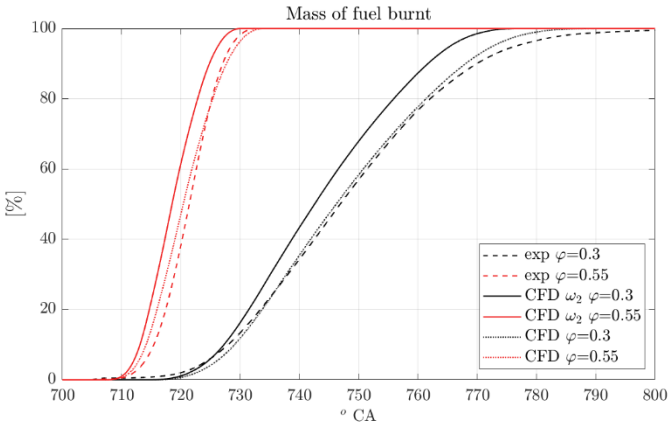

Figure 13. Numerical and experimental profiles of burnt fuel mass for the original framework and the one including the instability effect.

The effect of ω_2 appears to be beneficial only in the φ=0.55 case, as it brings the shape of heat release rate much closer to the experimental one, but at the cost of a shortening of the combustion initiation stage. This is quantitatively confirmed observing the combustion indicators reported in Figs. 14a), 14b) and 14c). In fact, the combustion duration (MFB 10-90) remains very close to the experimental one and the delay observed in the MFB50 is mainly generated in the combustion initiation (MFB 0-10).

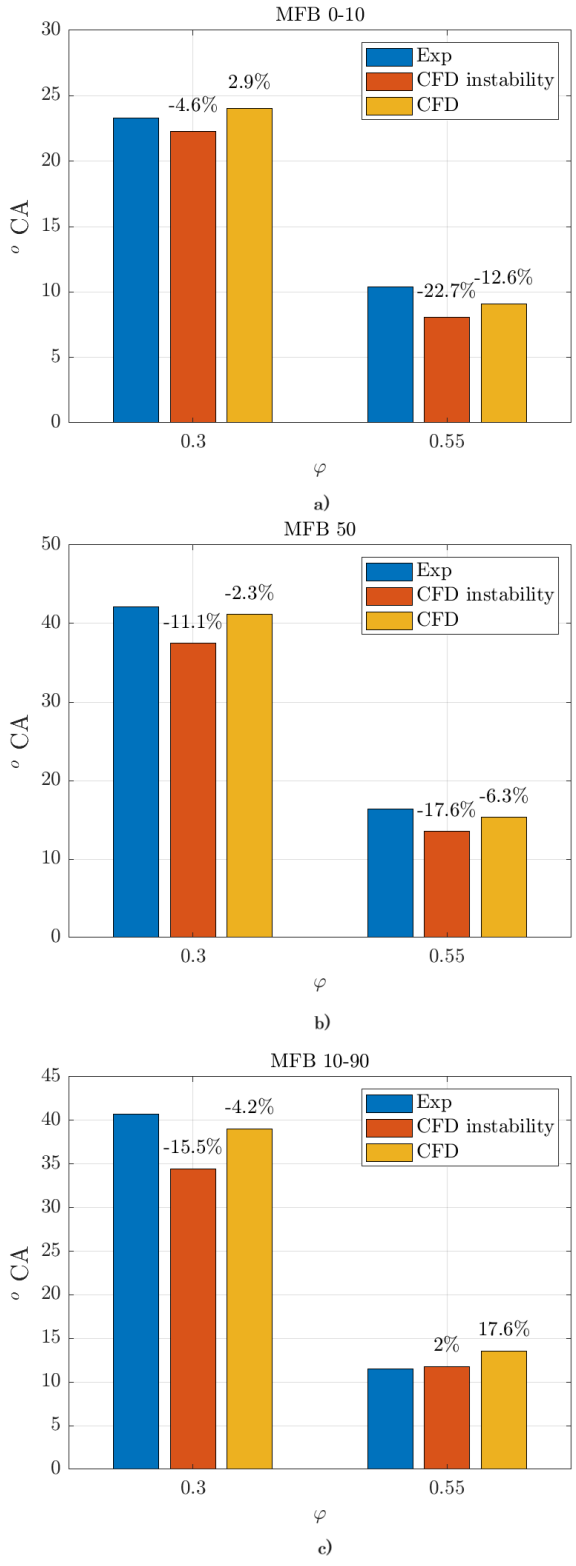

Figure 14. Experimental and numerical combustion durations 0-10 a), 50 b) and 10-90 c) for the framework including and not including instability acceleration.

As for the φ=0.3 case, it is overall worse. As visible in Fig. 13, the profile of burnt mass has a much steeper slope and despite the initiation is not far from experimental counterpart, the main duration is much shorter, leading to the end of the combustion many crank angles in advance. The underestimation of the combustion durations is greater and greater through the phases, as visible in Figs. 14a), 14b) and 14c).

However, before any conclusion, it is important to remember Bradley theory about the turbulence-instability interaction. In this regard, Fig. 15 shows the Karlovitz stretch factor as defined in Eq. 6 for the studied cases during combustion. Since φ=0.3 case is well over the limit of 0.1 observed by Bradley, it should not include the instability effect. On the contrary, φ=0.55 case should account for such an effect. In other words, at φ=0.3, original results should be kept. Conversely, at φ=0.55, new outcomes should be considered.

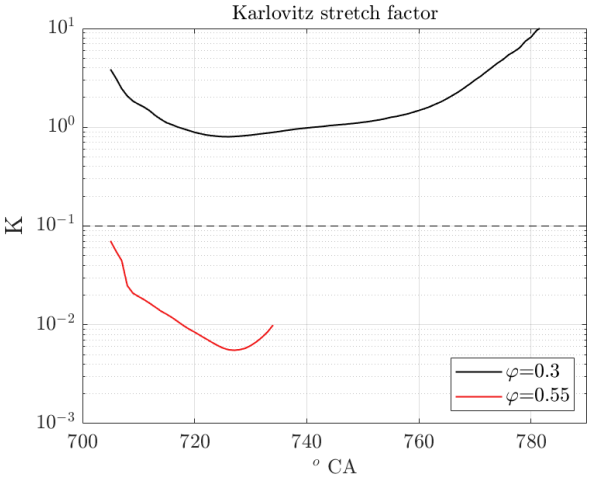

Figure 15. Average Karlovitz number on flame front during combustion progress for both studied cases.

In the light of all these considerations, it is possible to state that the ignition and combustion model calibrations employed in the past activities [11], [12], if paired with the thermo-diffusive instability correction, lead to an underestimation of the MFB 0-10 at φ=0.55 while, at φ=0.3, it is close to the experimental value. On the one hand, this means that a recalibration is needed. On the other hand, an excessive sensitivity of the kernel growth rate to the equivalence ratio is noticed.

SUMMARY/CONCLUSIONS

The work proposes a numerical framework to simulate ultra-lean hydrogen combustion in ICEs. The framework is investigated in two declinations, i.e. including or not a correction factor that considers the increased stretch due to thermo-diffusive instability effect.

In the leanest case, at φ=0.3, the addition of the correction does not lead to any modification. The reason is that, at these conditions, the instability effect is mitigated by the turbulence induced wrinkling, which prevails.

At φ=0.55, the thermo-diffusive instability effect improves the results, with apparent heat release rate and burnt mass profiles much closer to the experimental counterparts. Including the instability effect, the combustion duration (MFB 10-90) moves from an overestimation of 17.6% to a negligible error of 2%. However, such an improvement at φ=0.55 comes at the cost of a worsening of the combustion phasing. MFB 50 error increases from -6.3% to -17.6% considering the instability. However, most of this shift is accumulated at the start of the combustion. In fact, MFB 0-

10 shows an underestimation of 22.7%. Therefore, the ignition model should be modified to improve the φ=0.55 case, while keeping the φ=0.3 one unchanged. In other words, it should be recalibrated in order to reduce its sensitivity to the equivalence ratio.

Overall, it is evident that the thermo-diffusive instability should be carefully considered. In particular:

- in literature, only few evidences are available to prove the effectiveness of the adopted theories integrating the thermo-diffusive instability [8], [40];
- after including the instability effect, a specific recalibration of the cases is needed to highlight the benefit;
- concurrent effects as turbulence [38] or flame kernel size [23] can mitigate the instability-induced acceleration, thus they cannot be neglected.

REFERENCES

[1] C. Ramalho Leite, M. Laignel, P. Brequigny, J. Borée, and F. Foucher, "Experimental Combustion Analysis in a Gasoline Baseline Hydrogen-Fueled Internal Combustion Engine at Ultra-Lean Conditions," Aug. 2023. doi: 10.4271/2023-24-0073.

[2] Q. Luo *et al.*, "Experimental investigation of combustion characteristics and NOx emission of a turbocharged hydrogen internal combustion engine," *Int J Hydrogen Energy*, vol. 44, no. 11, pp. 5573–5584, Feb. 2019, doi: 10.1016/j.ijhydene.2018.08.184.

[3] A. Marwaha and K. A. Subramanian, "Experimental investigations of effects of cycle time on NOx emission in a hydrogen fueled multi-cylinder automotive spark ignition engine," *Sustainable Energy Technologies and Assessments*, vol. 52, p. 102203, Aug. 2022, doi: 10.1016/j.seta.2022.102203.

[4] T. Tsujimura and Y. Suzuki, "Development of a large-sized direct injection hydrogen engine for a stationary power generator," *Int J Hydrogen Energy*, vol. 44, no. 22, pp. 11355–11369, Apr. 2019, doi: 10.1016/j.ijhydene.2018.09.178.

[5] Q. Luo and B. Sun, "Experiments on the effect of engine speed, load, equivalence ratio, spark timing and coolant temperature on the energy balance of a turbocharged hydrogen engine," *Energy Convers Manag*, vol. 162, pp. 1–12, Apr. 2018, doi: 10.1016/j.enconman.2017.12.051.

[6] G. Maio *et al.*, "Experimental and numerical investigation of a direct injection spark ignition hydrogen engine for heavy-duty applications," *Int J Hydrogen Energy*, vol. 47, no. 67, pp. 29069–29084, Aug. 2022, doi: 10.1016/j.ijhydene.2022.06.184.

[7] F. Berni, V. Pessina, L. Teodosio, A. d'Adamo, M. Borghi, and S. Fontanesi, "An integrated 0D/1D/3D numerical framework to predict performance, emissions, knock and heat transfer in ICEs fueled with NH3–H2 mixtures: The conversion of a marine Diesel engine as case study," *Int J Hydrogen Energy*, Oct. 2023, doi: 10.1016/j.ijhydene.2023.09.158.

[8] I. Hernandez, C. Turquand D'Auzay, R. Penning, E. Shapiro, and J. Hughes, "Thermo-Diffusive Flame Speed Adjustment and its Application to Hydrogen Engines," in *SAE Technical Papers*, SAE International, Apr. 2023. doi: 10.4271/2023-01-0197.

[9] X. Liu *et al.*, "Hydrogen pre-chamber combustion at lean-burn conditions on a heavy-duty diesel engine: A computational study," *Fuel*, vol. 335, p. 127042, Mar. 2023, doi: 10.1016/j.fuel.2022.127042.

[10] R. Babayev, A. Andersson, A. S. Dalmau, H. G. Im, and B. Johansson, "Computational characterization of hydrogen direct injection and nonpremixed combustion in a compression-ignition engine," *Int J Hydrogen Energy*, vol. 46, no. 35, pp. 18678–18696, May 2021, doi: 10.1016/j.ijhydene.2021.02.223.

[11] S. Sfriso, F. Berni, S. Fontanesi, A. D'Adamo, M. Antonelli, and S. Frigo, "A 3D-CFD Numerical Approach for Combustion Simulations of Spark Ignition Engines Fuelled with Hydrogen: A Preliminary Analysis," Apr. 2023. doi: 10.4271/2023-01-0207.

[12] S. Sfriso *et al.*, "Proposal and validation of a numerical framework for 3D-CFD in-cylinder simulations of hydrogen spark-ignition internal combustion engines," *Int J Hydrogen Energy*, vol. 53, pp. 114–130, Jan. 2024, doi: 10.1016/j.ijhydene.2023.12.027.

[13] S. Sfriso *et al.*, "Proposal and Validation of 3D-CFD Framework for Ultra-Lean Hydrogen Combustion in ICEs," Apr. 2024. doi: 10.4271/2024-01-2685.

[14] V. Yakhot and S. A. Orszag, "Renormalization group analysis of turbulence. I. Basic theory," *J Sci Comput*, vol. 1, no. 1, pp. 3–51, 1986, doi: 10.1007/BF01061452.

[15] *STAR-CD methodology guide*.

[16] L. Teodosio and F. Berni, "Optimization via genetic algorithm of a variable-valve-actuation spark-ignition engine based on the integration between 1D/3D simulation codes and optimizer," *International Journal of Engine Research*, 2022, doi: 10.1177/14680874221099874.

[17] C. Iacovano, F. Berni, A. Barbato, and S. Fontanesi, "A Preliminary 1D-3D Analysis of the Darmstadt Research Engine under Motored Condition," in *E3S Web of Conferences*, EDP Sciences, Oct. 2020. doi: 10.1051/e3sconf/202019706006.

[18] F. Berni, G. Cicalese, M. Borghi, and S. Fontanesi, "Towards grid-independent 3D-CFD wall-function-based heat transfer models for complex industrial flows with focus on in-cylinder simulations," *Appl Therm Eng*, vol. 190, May 2021, doi: 10.1016/j.applthermaleng.2021.116838.

[19] F. Berni, G. Cicalese, S. Sparacino, and G. Cantore, "On the existence of universal wall functions in in-cylinder simulations using a low-Reynolds RANS turbulence model," in *AIP Conference Proceedings*, American Institute of Physics Inc., Dec. 2019. doi: 10.1063/1.5138752.

[20] A. d'Adamo, C. Iacovano, and S. Fontanesi, "Large-Eddy simulation of lean and ultra-lean combustion using advanced ignition modelling in a transparent combustion chamber engine," *Appl Energy*, vol. 280, Dec. 2020, doi: 10.1016/j.apenergy.2020.115949.

[21] R. Herweg and R. R. Maly, "A Fundamental Model for Flame Kernel Formation in S. I. Engines," Oct. 1992. doi: 10.4271/922243.

[22] H. K. Versteeg and W. Malalasekera, "An Introduction to Computational Fluid Dynamics Second Edition." [Online]. Available: www.pearsoned.co.uk/versteeg

[23] D. Bradley, M. Lawes, K. Liu, S. Verhelst, and R. Woolley, "Laminar burning velocities of lean hydrogen–air mixtures at pressures up to 1.0 MPa," *Combust Flame*, vol. 149, no. 1–2, pp. 162–172, Apr. 2007, doi: 10.1016/j.combustflame.2006.12.002.

[24] A. A. Konnov, "On the role of excited species in hydrogen combustion," *Combust Flame*, vol. 162, no. 10, pp. 3755–3772, Oct. 2015, doi: 10.1016/j.combustflame.2015.07.014.

[25] "DARS Manual - Book 4".

[26] S. Verhelst, C. TJoen, J. Vancoillie, and J. Demuynck, "A correlation for the laminar burning velocity for use in hydrogen spark ignition engine simulation," *Int J Hydrogen Energy*, vol. 36, no. 1, pp. 957–974, Jan. 2011, doi: 10.1016/j.ijhydene.2010.10.020.

[27] V. L. Zimont, "Gas premixed combustion at high turbulence. Turbulent flame closure combustion model," *Exp Therm Fluid Sci*, vol. 21, no. 1–3, pp. 179–186, Mar. 2000, doi: 10.1016/S0894-1777(99)00069-2.

[28] A. N. Lipatnikov and J. Chomiak, "Turbulent flame speed and thickness: phenomenology, evaluation, and application in multi-dimensional simulations," *Prog Energy Combust Sci*, vol. 28, no. 1, pp. 1–74, Jan. 2002, doi: 10.1016/S0360-1285(01)00007-7.

[29] Ö. L. Gülder, "Turbulent premixed flame propagation models for different combustion regimes," *Symposium (International) on Combustion*, vol. 23, no. 1, pp. 743–750, Jan. 1991, doi: 10.1016/S0082-0784(06)80325-5.

[30] Konnov AA, "Refinement of the kinetic mechanism of hydrogen combustion," *Adv Chem Phys*, vol. 23, pp. 5–18, 2004.

[31] M. Matalon, "The Darrieus-Landau instability of premixed flames," *Fluid Dyn Res*, vol. 50, no. 5, Aug. 2018, doi: 10.1088/1873-7005/aab510.

[32] T. L. Howarth and A. J. Aspden, "An empirical characteristic scaling model for freely-propagating lean premixed hydrogen flames," *Combust Flame*, vol. 237, p. 111805, Mar. 2022, doi: 10.1016/j.combustflame.2021.111805.

[33] T. L. Howarth, E. F. Hunt, and A. J. Aspden, "Thermodiffusively-unstable lean premixed hydrogen flames: Phenomenology, empirical modelling, and thermal leading points," *Combust Flame*, vol. 253, p. 112811, Jul. 2023, doi: 10.1016/j.combustflame.2023.112811.

[34] C. K. Law and C. J. Sung, "Structure, aerodynamics, and geometry of premixed flamelets," *Prog Energy Combust Sci*, vol. 26, no. 4–6, pp. 459–505, Aug. 2000, doi: 10.1016/S0360-1285(00)00018-6.

[35] N. Fogla, F. Creta, and M. Matalon, "Effect of folds and pockets on the topology and propagation of premixed turbulent flames," *Combust Flame*, vol. 162, no. 7, pp. 2758–2777, Jul. 2015, doi: 10.1016/j.combustflame.2015.04.012.

[36] A. S. AL-SHAHRANY, D. BRADLEY, M. LAWES, K. LIU, and R. WOOLLEY, "DARRIEUS–LANDAU AND THERMO-ACOUSTIC INSTABILITIES IN CLOSED VESSEL EXPLOSIONS," *Combustion Science and Technology*, vol. 178, no. 10–11, pp. 1771–1802, Dec. 2006, doi: 10.1080/00102200600788734.

[37] D. Bradley, P. H. Gaskell, X. J. Gu, and A. Sedaghat, "Premixed flamelet modelling: Factors influencing the turbulent heat release rate source term and the turbulent burning velocity," *Combust Flame*, vol. 143, no. 3, pp. 227–245, Nov. 2005, doi: 10.1016/j.combustflame.2005.05.014.

[38] D. Bradley, M. Lawes, K. Liu, and M. S. Mansour, "Measurements and correlations of turbulent burning velocities over wide ranges of fuels and elevated pressures," *Proceedings of the Combustion Institute*, vol. 34, no. 1, pp. 1519–1526, 2013, doi: 10.1016/j.proci.2012.06.060.

[39] G. Cicalese, F. Berni, and S. Fontanesi, "Integrated in-cylinder / CHT methodology for the simulation of the engine thermal field: An application to high performance turbocharged DISI engines," *SAE Int J*

Engines, vol. 9, no. 1, pp. 601–617, Apr. 2016, doi: 10.4271/2016-01-0578.

[40] V. De Bellis *et al.*, "Development and validation of a phenomenological model for hydrogen fueled PFI internal combustion engines considering Thermo-Diffusive effects on flame speed propagation," *Energy Convers Manag*, vol. 308, p. 118395, May 2024, doi: 10.1016/j.enconman.2024.118395.

CONTACT INFORMATION

Dr. Stefano Sfriso
Internal combustion engine research group
University of Modena and Reggio Emilia
Phone number +39 0592056114
stefano.sfriso@unimore.it

ACKNOWLEDGMENTS

The experimental work described in this paper has been conducted by Caio Ramalho Leite and Fabrice Foucher from the University of Orléans.

The authors gratefully acknowledge the University of Modena and Reggio Emilia for supporting the activity by the "Fondo di Ateneo per la Ricerca 2023 per il finanziamento di piani di sviluppo dipartimentale nell'ambito della ricerca" (FAR 2023), the Agence Nationale de Recherche for the grant number 20-CE05-0007 (ALEKCIA ANR project) and the "PIANO NAZIONALE DI RIPRESA E RESILIENZA (PNRR) – MISSIONE 4 COMPONENTE 2, "Dalla ricerca all'impresa" INVESTIMENTO 1.4, Potenziamento strutture di ricerca e creazione di "campioni nazionali di R&S" su alcune Key Enabling Technologies, finanziato dall'Unione europea – NextGenerationEU - Progetto identificato con codice CN00000023. Titolo "Sustainable Mobility Center (Centro Nazionale per la Mobilità Sostenibile – CNMS)" - Spoke 12 - Avviso MUR 3138/2021 modificato con DD 3175/2021".

DEFINITIONS/ABBREVIATIONS

A	Empirical coefficient for turbulent flame speed calibration
AHRR	Apparent heat release rate
A_k	Flame kernel area
B	Factor for turbulent transition of flame kernel
BDC	Bottom Dead Center
bTDC	Before top dead center
C	Factor for turbulent transition of flame kernel
CA	Crank Angle
CFD	Computational fluid dynamics
CHT	Conjugate heat transfer
CoV	Coefficient of variation
c_p	Specific heat at constant pressure
DISI	Direct injection spark ignition
ECFM	Extended coherent flamelet model
EGR	Exhaust gas recirculation
ICE	Internal combustion engine
Id	Ignition distance
IMEP	Indicated mean effective pressure
K	Karlovitz stretch factor
k	Heat conductivity
Le_{eff}	Effective Lewis number
l_t	Turbulence integral length scale
MFB	Mass of fuel burnt
p	Pressure
PFI	Port fuel injection
Pr	Prandtl number
Q	Heat
RANS	Reynolds averaged Navier Stokes
R_l	Turbulent Reynolds number
r_k	Flame kernel radius
S	Source term for heat conduction equation

S_{cond}	Flame kernel expansion contribution due to heat conduction
SI	Spark Ignition
Sl	Laminar Flame Speed
Sl_{Corr}	Corrected Laminar Flame Speed
S_T	Turbulent Flame Speed
T	Temperature
t	Time
tg	Time constant
TJI	Turbulent jet ignition
T_k	Flame kernel temperature
tke	Turbulent kinetic energy
trel	Time passed after ignition
T_u	Unburnt temperature
u'	Turbulent velocity Fluctuations
u_l	Laminar burning velocity
Umean	Mean flow velocity
V	Volume
V_k	Flame kernel volume
x	Space coordinate
β	Zel'dovich number
δ_l	Laminar flame thickness
φ	Equivalence ratio
φ_{lim}	Limit equivalence ratio
γ	Specific heat ratio
$\varkappa$	Flame curvature
ν	Dynamic viscosity
ρ	Density
ρ_u	Unburnt gases density
ω	Instability growth rate
ω_{dl}	First order term of instability growth rate